Cancer Research

Novel Androgen Receptor Coregulator GRHL2 Exerts Both Oncogenic and Antimetastatic Functions in Prostate Cancer

Steve Paltoglou[1,2], Rajdeep Das[1,2], Scott L. Townley[1,2], Theresa E. Hickey[1,2], Gerard A. Tarulli[1,2], Isabel Coutinho[1,2], Rayzel Fernandes[1,2], Adrienne R. Hanson[1,2], Iza Denis[1,2], Jason S. Carroll[3], Scott M. Dehm[4,5], Ganesh V. Raj[6], Stephen R. Plymate[7], Wayne D. Tilley[1,2], and Luke A. Selth[1,2]

Abstract

Alteration to the expression and activity of androgen receptor (AR) coregulators in prostate cancer is an important mechanism driving disease progression and therapy resistance. Using a novel proteomic technique, we identified a new AR coregulator, the transcription factor Grainyhead-like 2 (GRHL2), and demonstrated its essential role in the oncogenic AR signaling axis. GRHL2 colocalized with AR in prostate tumors and was frequently amplified and upregulated in prostate cancer. Importantly, GRHL2 maintained AR expression in multiple prostate cancer model systems, was required for cell proliferation, enhanced AR's transcriptional activity, and colocated with AR at specific sites on chromatin to regulate genes relevant to disease progression. *GRHL2* is itself an AR-regulated gene, creating a positive feedback loop between the two factors. The link between GRHL2 and AR also applied to constitutively active truncated AR variants (ARV), as GRHL2 interacted with and regulated ARVs and vice versa. These oncogenic functions of GRHL2 were counterbalanced by its ability to suppress epithelial–mesenchymal transition and cell invasion. Mechanistic evidence suggested that AR assisted GRHL2 in maintaining the epithelial phenotype. In summary, this study has identified a new AR coregulator with a multifaceted role in prostate cancer, functioning as an enhancer of the oncogenic AR signaling pathway but also as a suppressor of metastasis-related phenotypes. *Cancer Res; 77(13); 3417–30. ©2017 AACR.*

Introduction

Prostate cancer is the most frequent male non-skin cancer and a major cause of cancer-associated death. Prostate cancer growth and survival is driven by androgen receptor (AR) activation in response to ligand (androgen) binding. Accordingly, androgen deprivation therapy (ADT) is the first-line treatment for locally advanced and metastatic disease. However, resistance to ADT and disease progression, termed castrate-resistant prostate cancer (CRPC), is inevitable. The recent success of second-generation ADT agents (i.e., the AR antagonist enzalutamide and the androgen synthesis inhibitor abiraterone acetate) in achieving a survival benefit in men with CRPC highlights an ongoing dependence on AR signaling in this disease setting (1). Unfortunately, even these new, more potent, drugs are only palliative, with a mean average survival benefit measured in months, and the resultant disease generally remains AR-driven (1).

Mechanisms underlying continued AR activity in CRPC include deregulation of androgen biosynthesis and direct changes to the AR, including gene amplification, gain-of-function mutations, and the emergence of constitutively active truncated AR variants (ARV) that lack a functional ligand-binding domain (2). Another adaptive response that can mediate AR signaling in the castrate environment is altered expression and activity of AR coregulator proteins. Over 130 AR coregulators have been identified, comprising a highly complex system for shaping AR function in the normal and malignant prostate (3). In general, CRPC is characterized by gain of coactivators and loss of corepressors, which collectively enhances AR signaling in the castrate environment.

Here, we utilized an unbiased proteomics technique, termed rapid immunoprecipitation mass spectrometry of endogenous proteins (RIME; ref. 4), to elucidate the chromatin-associated AR interactome. We identified a novel AR-associated factor, Grainyhead-like 2 (GRHL2), and demonstrated that it plays a major role in maintaining AR expression and signaling in prostate cancer while simultaneously suppressing metastasis-associated phenotypes.

[1]Dame Roma Mitchell Cancer Research Laboratories, Adelaide Medical School, The University of Adelaide, South Australia, Australia. [2]Freemasons Foundation Centre for Men's Health, Adelaide Medical School, The University of Adelaide, South Australia, Australia. [3]Cancer Research UK Cambridge Research Institute, Li Ka Shing Centre, Robinson Way, Cambridge, United Kingdom. [4]Masonic Cancer Center, University of Minnesota, Minneapolis, Minnesota. [5]Department of Laboratory Medicine and Pathology, University of Minnesota, Minneapolis, Minnesota. [6]Department of Urology, University of Texas Southwestern Medical Center, Dallas, Texas. [7]Department of Medicine and VAPSHCS, University of Washington, Seattle, Washington.

Note: Supplementary data for this article are available at Cancer Research Online (http://cancerres.aacrjournals.org/).

Corresponding Author: Luke A. Selth, The University of Adelaide, PO Box 14, Rundle Mall, Adelaide, SA 5000, Australia. Phone: 618-8222-3618; Fax: 618-222-3217; E-mail: luke.selth@adelaide.edu.au

doi: 10.1158/0008-5472.CAN-16-1616

Materials and Methods

Cell line culture and transfection

R1-AD1 and R1-D567 have been described previously (5). C4-2B, LNCaP, VCaP, 22Rv1, PC3, and DU145 human prostate carcinoma cells were obtained from the ATCC. Cells were cultured as described previously (6). The number of passages between thawing cell lines and their use in the described experiments were as follows: R1-AD1, R1-D567, and 22Rv1 (passages 2–30); C4-2B and PC3 (2–15); LNCaP (2–20); VCaP (2–8); DU145 (2–10). All cell lines underwent (i) verification by short-tandem repeat profiling in July or August 2016 by CellBank Australia and (ii) regular (approximately every 4 months) testing using a custom PCR-based assay to ensure lack of contamination with the most common *Mycoplasma* and *Acholeplasma* strains.

Cells were transfected with 20 nmol/L siRNA using RNAiMAX transfection reagent (Life Technologies), according to the manufacturer's instructions. The following siRNAs were used in this study: GRHL2 (sc77606a, sc77606b, and sc77606c; Santa Cruz Biotechnology) and AR (AR Silencer 51539, #4390826; Ambion). For transfecting cells with the GRHL2 expression plasmid (pCMV-NEO-GRHL2, #SC305189; Origene Technologies), we used Lipofectamine 2000 (Life Technologies).

Stable LNCaP-shGRHL2 cell lines were generated using GRHL2-specific shRNA plasmids (TRCN0000015808 and TRCN0000015810) and an shRNA control plasmid (Shc002) from Sigma as described previously (7).

Rapid immunoprecipitation mass spectrometry of endogenous proteins

RIME was carried out essentially as described (4). A total of 3×10^7 R1-AD1 cells or 6×10^7 R1-D567 cells were subjected to immunoprecipitation with 10 μg of AR antibody (Santa Cruz Biotechnology, AR N20; sc-816). Only coprecipitating proteins that occurred in 3 of 3 independent biological replicates were considered, and further filtering was achieved by excluding proteins that appeared in >1 of the 3 matching IgG controls.

Coimmunoprecipitation

R1-AD1 and R1-D567 cells were seeded at 2.5×10^6 cells/plate and LNCaP cells were seeded at 3.0×10^6 cells/plate in RMPI 1640 +10% CSS. After 72 hours, media were replaced with fresh RPMI 1640 + 10% CSS containing 10 nmol/L DHT. After an additional 4 hours, nuclear pellets were made according to the RIME protocol. Nuclear pellets were sonicated for 10 cycles (30 seconds on, 30 seconds off) using a Diagenode Bioruptor. After centrifugation, lysates were immunoprecipitated overnight with 5 μg AR antibody (Santa Cruz Biotechnology; #sc-816x) or 5 μg of GRHL2 antibody (Sigma HPA004820) precoupled to Protein G Dynabeads (Life Technologies; 10004D). The following day, the beads were washed 3 times with PBS and then boiled in SDS-PAGE sample buffer, prior to analysis by Western blotting.

Analysis of GRHL2 expression in published datasets

Transcriptomic data were downloaded from GEO (GSE35988 and GSE21032), The Cancer Genome Atlas (TCGA) data portal, and cBioPortal (8). *GRHL2* copy-number data were obtained via cBioPortal (8).

Western blotting and antibodies

Protein extraction from cells, using RIPA buffer and Western blotting, was done as described previously (9). Antibodies used in Western blotting were as follows: AKT1/2 (Santa Cruz Biotechnology; N-19; sc-1619); pAKT (Cell Signaling Technology; Thr308, #9275S); AR (Santa Cruz Biotechnology; N20; sc-816); E-Cadherin (BD Biosciences; clone 36/E); ERK1 (Santa Cruz Biotechnology; K23; sc-94); pERK (Cell Signaling Technology; Thr202/Tyr204, #9101); GRHL2 (Sigma; HPA004820); GAPDH (EMD Millipore; MAB374); N-cadherin (Santa Cruz Biotechnology; H-63; sc-7939); Tubulin (EMD Millipore; 05-829); vimentin (Abcam EPR3776); ZEB1 (Santa Cruz Biotechnology; H102; Sc-25388); and ZO-1 (Cell Signaling, D7D12).

Quantitative real-time PCR

RNA extraction from cells, using TRIzol reagent and RT-qPCR, was done as described previously (9). *GAPDH* was used for normalization of RT-qPCR data. Fold changes in mRNA expression levels were calculated using the comparative C_t method as described. Primer sequences are available on request.

Immunofluorescence

Four μm sections of paraffin-embedded human transurethral resection of the prostate tumor samples were cut and adhered to Superfrost Ultra Plus–coated slides (Menzel-Glaser) overnight at 45°C, then de-waxed and immunolabeled as previously described (10). Primary antibodies [1:400 rabbit anti-GRHL2 (Sigma HPA004820) or 1:60 mouse anti-AR (Dako M3562)] were incubated overnight at 4°C and secondary antibodies [goat anti-mouse AlexaFluor 488 (Thermo A-11029) or goat anti-rabbit Alexa 594 (Thermo A-11037)] incubated for 30 minutes at room temperature. Images were acquired on a Zeiss 700 confocal microscope. Two-dimension expression intensity histograms and Spearman's correlation coefficients were generated using ImageJ software and the Coloc2 plugin.

IHC

IHC for GRHL2 was carried out as described (11) using anti-GRHL2 antibody (Sigma HPA004820) at a 1:8,000 dilution. Slide digitization, annotation, and immunohistochemical quantification were done as described (12).

Transactivation assays

Transactivation assays with the probasin luciferase reporter construct were carried out essentially as described previously (13), with the exception that cells were cotransfected with 1 ng of pCMV-NEO-GRHL2 plasmid, 1 ng of pcDNA-AR, 1 ng of pRL-CMV, and 100 ng of the probasin reporter construct.

Chromatin immunoprecipitation and ChIP-seq

LNCaP cells were seeded at 3×10^6 cells/plate in 15 cm plates in RPMI 1640 + 10% FBS and allowed to grow for 3 days prior to fixation. Chromatin immunoprecipitation (ChIP) was then performed as described previously (14). For ChIP-qPCR, 2 μL of DNA was used in 10 μL PCR reactions. For ChIP-seq, 5 ng of DNA (ChIP-enriched or input) was used for library creation with a Illumina TruSeq ChIP Library Prep kit (Illumina) and sequenced (75 bp single-end reads) at the South Australian Health and Medical Research Institute Genomics Facility using an Illumina NextSeq 500. Mapping of sequencing data and

peak calling (using input DNA as a control) were performed as described previously (6). Consensus peaks were determined by including only regions identified in two biological replicates. ChIP-seq data are available through NCBI's Gene Expression Omnibus (GSE80256).

To identify AR/GRHL2 shared binding regions, ChIPpeakAnno (implemented in R 2.12.0; ref. 15) was used with a maxgap value of 1000. Cistrome (16) was used to generate heatmaps. HOMER (17) was used to generate histograms of tag density around peaks. Regions of AR/GRHL2 binding were annotated with respect to neighboring genes ($\leq$50 kb from the transcription start site) using CisGenome (18). Identification of enriched sequence motifs (known and *de novo*) was performed as described previously (19). Visualization of ChIP-seq data was performed using Integrated Genomics Viewer (IGV 2.3, Broad Institute; ref. 20).

Our AR/GRHL2 ChIPSeq data were also compared with other published datasets: H3K4me2, H3K4me3, H3K27ac, P300, MED12, and FoxA1 from Wang and colleagues (21); H3K9me3 and H3K27me3 from Yu and colleagues (22); and RNAPII from He and colleagues (23). Read data from these studies were downloaded and mapped around AR and GRHL2 peaks sets using HOMER.

RNA sequencing

RNA from LNCaP cells was prepared using Trizol 2 days after transfection with siGRHL2. Libraries were generated using 10 ng of RNA and NEXTflex Rapid Illumina Directional RNA-Seq Library Prep Kits (Bioo Scientific), according to the manufacturer's instructions. Sequencing was carried out at the South Australian Health and Medical Research Institute Genomics Facility using an Illumina NextSeq 500 (75 bp single-end reads). Reads were mapped using TopHat v2.0.9 (24) in Galaxy (25, 26), using default parameters and hg19 as the reference genome. Raw counts per exon (mapped to hg19_genes_2012-03-09.gtf) were estimated using htseq-count (27). Subsequently, DESeq2 (implemented in Bioconductor v2.12, R v3.0.1; ref. 28) was used to identify differentially expressed genes. RNA sequencing (RNA-seq) data are available through NCBI's Gene Expression Omnibus (GSE80452).

For gene set enrichment analysis (GSEA; ref. 29), read counts were normalized using the DESeq2 rlog transformation algorithm, genes were ranked using a signal to noise metric, and the GSEAPreranked tool was run on the GenePattern server (http://www.broad.mit.edu/tools/software.html). A signature of GRHL2 activity was made by considering the top 100 differentially expressed genes in response to siGRHL2 knockdown (comprising 21 upregulated genes and 79 downregulated genes): GRHL2 activity scores for individual tumors from two large clinical cohorts were determined as described previously (23).

Chick chorioallantoic membrane assays

Chick chorioallantoic membrane (CAM) assays were approved by the University of Adelaide Animal Ethics Committee (approval number M-2014_079) and done using the *in ovo* method as described previously (7).

Statistical analyses

All statistical analyses were carried out using GraphPad Prism (version 5; GraphPad Software). Details of statistical tests used are provided in the figure legends.

Results

GRHL2 is a novel AR-interacting protein

To identify novel proteins that interact with AR and ARVs, we conducted RIME in R1-AD1 and R1-D567 cells. R1-D567 has been engineered such that AR exons 5 to 7 are deleted from the genome, leading to exclusive expression of the constitutively active ARv567es variant, whereas the R1-AD1 cell line expresses full-length AR only (5). RIME identified 54 and 75 proteins associated with AR and ARv567es, respectively (Supplementary Table S1). Analysis of the interactomes at the individual protein (Supplementary Table S1) and pathway (Fig. 1A) level revealed high concordance between ligand-activated AR and ARv567es. AR itself was isolated with high confidence, and many known AR coregulators, including FoxA1, P300, AP-1, and members of the SWI/SNF chromatin remodeling complex, were also identified in the interactomes, highlighting the robustness of the data.

Of the novel coprecipitating factors, the transcription factor GRHL2 was one of the most confident hits from both cell line models (Fig. 1B). AR only bound GRHL2 robustly in androgen-replete conditions, whereas, as expected, the constitutively active ARv567es variant interacted with GRHL2 in an androgen-independent manner (Fig. 1B). The interaction was confirmed by coimmunoprecipitation of GRHL2 using an AR antibody in R1-AD1, R1-D567, and LNCaP cells (Fig. 1C). A robust association between AR and GRHL2 in LNCaP cells was also evident by "reverse" coimmunoprecipitation (i.e., coimmunoprecipitation of AR with a GRHL2 antibody; Fig. 1D).

GRHL2 is commonly amplified and overexpressed in prostate cancer

To assess the clinical relevance of GRHL2 in prostate cancer, we examined a series of published cohorts for GRHL2 alterations (30–32). *GRHL2* resides at 8q.22.3, a genomic locus that is frequently amplified in prostate cancer: indeed, *GRHL2* gene copy number was gained/amplified in 54% to 71% of metastatic samples and 14% to 32% of primary tumors (Fig. 2A), and this alteration was associated with a trend toward increased *GRHL2* mRNA expression in CRPC (Fig. 2B). Moreover, *GRHL2* mRNA was elevated in malignant compared with nonmalignant prostate tissues (Fig. 2C) and was higher in Gleason score 8–10 versus Gleason 6 tumors (Fig. 2D).

Extending upon the *in silico* analyses, we used immunohistochemistry to evaluate GRHL2 protein expression in 101 matched nonmalignant prostate tissues and tumors. GRHL2 was detectable in all samples: staining was primarily nuclear and present in luminal epithelial cells, with minimal signal in the stroma. Representative images from strongly positive samples are shown in Fig. 2E (left). Although staining was strong in benign prostate samples (median staining index = 3.66), levels of GRHL2 were significantly higher in tumors (4.26; Fig. 2E, right). However, GRHL2 expression was not associated with other clinicopathologic parameters such as Gleason grade/score or serum prostate-specific antigen levels (data not shown).

To determine the potential for functional interaction between AR and GRHL2 in clinical specimens, we examined their tissue localization using dual immunofluorescence in human prostate tumors obtained from transurethral resections. Two representative sections are shown in Fig. 2F. AR and GRHL2 were primarily expressed in luminal epithelial cells. Although most cells

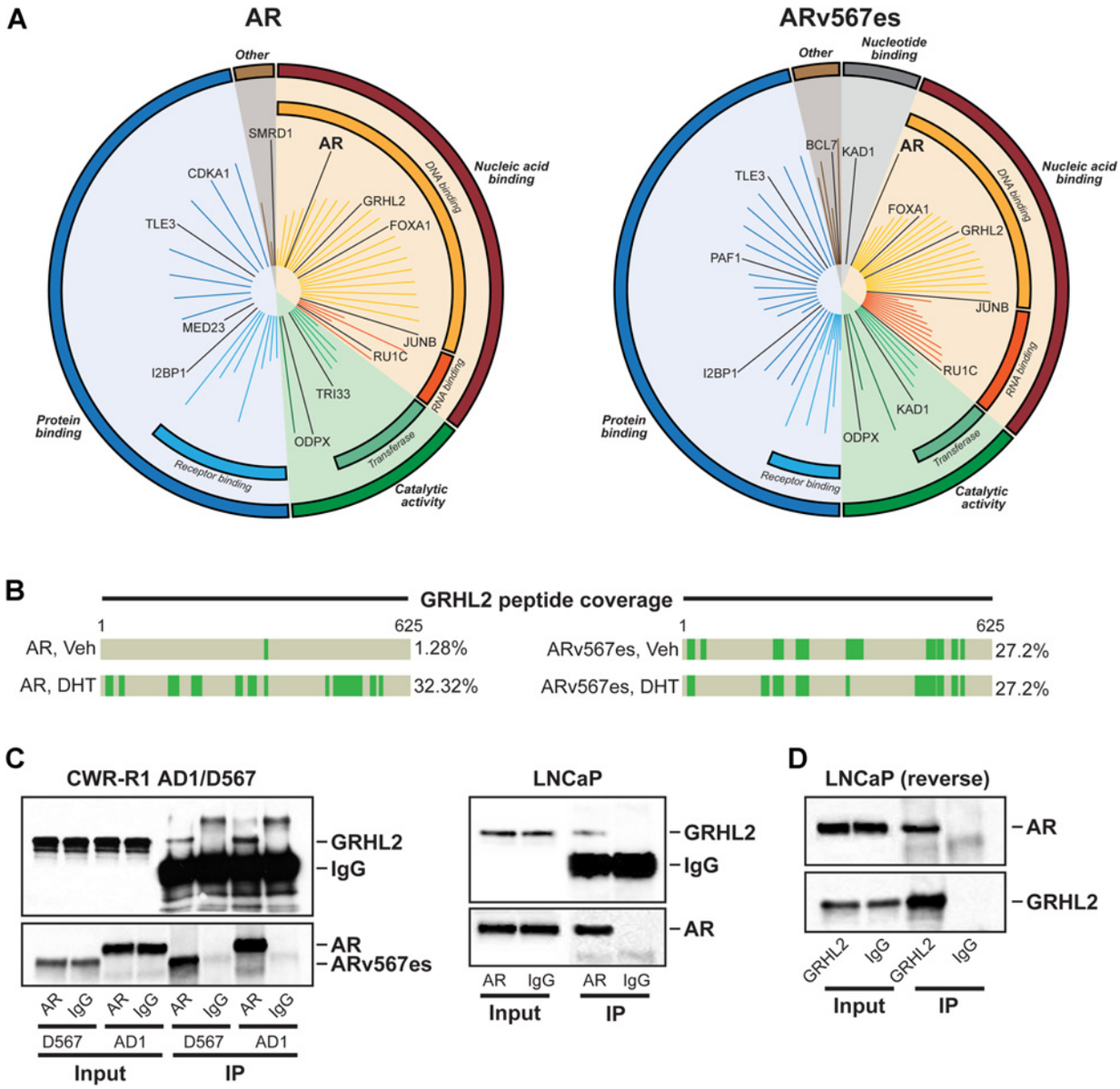

Figure 1.

GRHL2 is a novel AR-interacting protein. **A,** Graphical plots (generated by MS-ARC) showing AR- and ARv567es-associated proteins, clustered according to molecular function. The length of the line represents the Mascot score. **B,** Peptide coverage of GRHL2 from RIME experiments. **C** and **D,** Validation of AR:GRHL2 interaction by coimmunoprecipitation. AR protein in R1-AD1 and R1-D567 cells (left) and LNCaP cells (right) was immunoprecipitated and GRHL2 was detected by immunoblotting (**C**). GRHL2 protein in LNCaP cells was immunoprecipitated and AR was detected by immunoblotting (**D**). For all coimmunoprecipitations, IgG served as a negative control.

exhibited positivity for both factors, cells with high GRHL2 staining and low/no AR staining were evident. Using software to assess colocalization (see Materials and Methods), a high positive correlation between the expression of AR and GRHL2 was observed at the cellular level (Fig. 2F and Supplementary Fig. S1).

GRHL2 is an AR target gene

To identify appropriate model systems to characterize GRHL2 function, its expression was assessed in a panel of prostate cancer cell lines. GRHL2 was most highly expressed in VCaP cells and not detectable in AR-negative PC3 or DU145 cells (Fig. 3A, left). This expression pattern closely mirrored that of AR (Fig. 3A, right), leading us to postulate that GRHL2 is an androgen-regulated factor. Supporting this idea, *GRHL2* mRNA levels were significantly induced by DHT treatment in multiple cell lines (Fig. 3B). This regulation was dependent on the AR, because siRNA-mediated AR knockdown cells led to a dramatic loss of GRHL2 protein in both

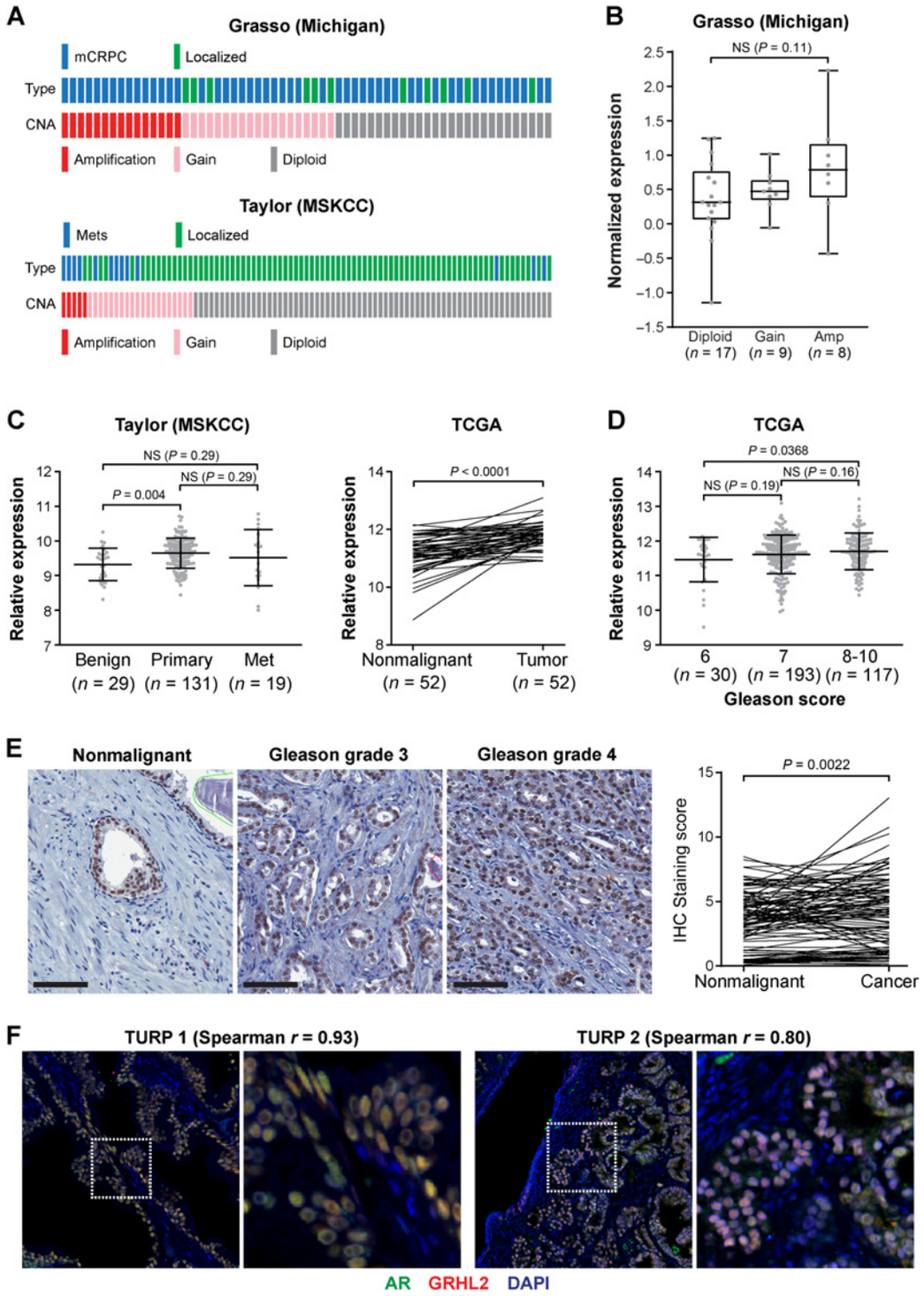

Figure 2.

GRHL2 is commonly amplified and overexpressed in prostate cancer. **A,** Oncoprints representing *GRHL2* copy-number alterations from the Grasso and Taylor datasets were generated using cBioPortal. mCRPC, metastatic castration-resistant prostate cancer; Mets, metastases. **B,** *GRHL2* gene amplification in the Grasso cohort is associated with increased mRNA expression. Boxes show minimum and maximum (bottom and top lines, respectively) and mean (line within the boxes) values. *P* value was determined an unpaired *t* test. **C,** *GRHL2* expression is elevated in primary prostate cancer. In the Taylor graph, lines represent the mean ± SD. *P* values were determined using unpaired (Taylor) or paired (TCGA) *t* tests. **D,** *GRHL2* expression is associated with Gleason grade. Lines in the graph represent the mean ± SD. *P* values were determined using unpaired *t* tests. **E,** Representative staining of nonmalignant and cancer tissues is shown on the left (bar, 100 μm). A graph of staining scores is shown on the right. *P* value was determined using a paired *t* test. **F,** Cellular coexpression of GRHL2 and AR in prostate tissues, as demonstrated by dual immunofluorescence. Shown are two representative prostate tumors. Nuclei were stained with DAPI. Spearman *r* values represent the correlation between AR and GRHL2 staining (see Materials and Methods). Scale bars, 50 μm.

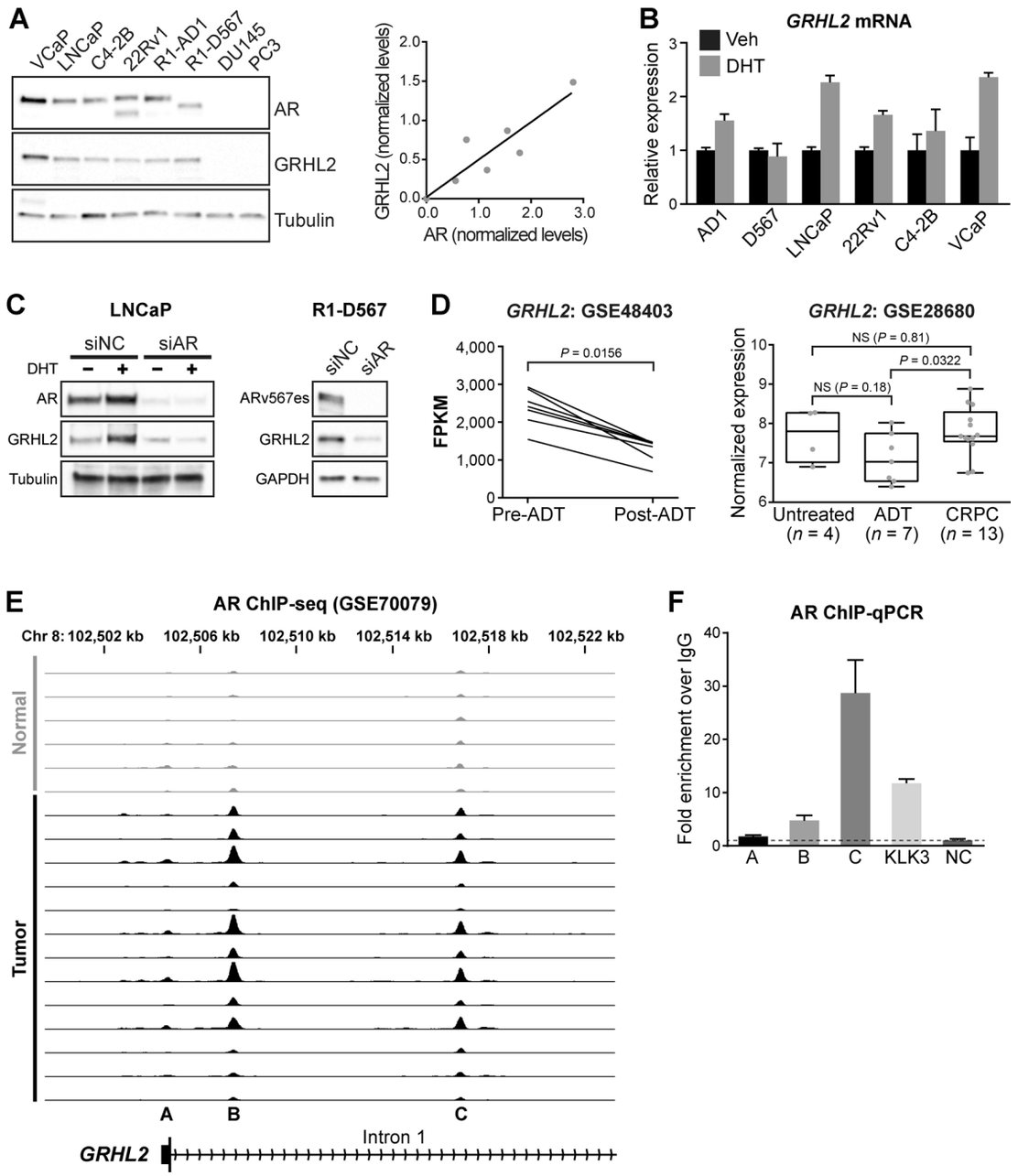

Figure 3.

Regulation of GRHL2 expression by AR in prostate cancer. **A,** GRHL2 protein levels in a panel of prostate cancer cell lines (tubulin is the loading control). The graph on the right shows the correlation between tubulin-normalized AR and GRHL2 in all cell lines. **B,** Cell lines were treated with 1 nmol/L DHT for 4 hours, and *GRHL2* levels were assessed by RT-qPCR. Error bars, ± SD. **C,** LNCaP (left) or R1-D567 (right) cells were transfected with siRNA targeting AR (siAR) or control siRNA (siNC) for 48 hours. LNCaP cells were additionally treated with 1 nmol/L DHT (or ethanol as a control) for 24 hours. Tubulin or GAPDH are loading controls. **D,** *GRHL2* mRNA expression in two clinical cohorts. Boxes in the right graph show minimum and maximum (bottom and top lines, respectively) and mean (line within the boxes) values. *P* values were determined using a Wilcoxon matched-pairs signed rank test (GSE48403) or unpaired *t* tests (GSE28680). FPKM, fragments per kilobase of exon per million mapped reads; NS, not significant. **E,** AR binding sites (from ChIP-seq) proximal to the GRHL2 gene in nonmalignant and prostate tumor samples (35). Each track depicts ChIP-seq AR binding intensity for a given sample. **F,** Validation of three putative AR binding sites (**A–C**; shown below the ChIP-seq tracks in **E**) by ChIP-qPCR. Error bars, ± SEM.

the presence and absence of androgen (Fig. 3C, left). Using the R1-D567 cell line model, we demonstrated that GRHL2 is also regulated by the constitutively-active ARV, ARv567es. In support of the *in vitro* data, *GRHL2* expression decreased following ADT and was regained in CRPC in clinical specimens (Fig. 3D; refs. 33, 34).

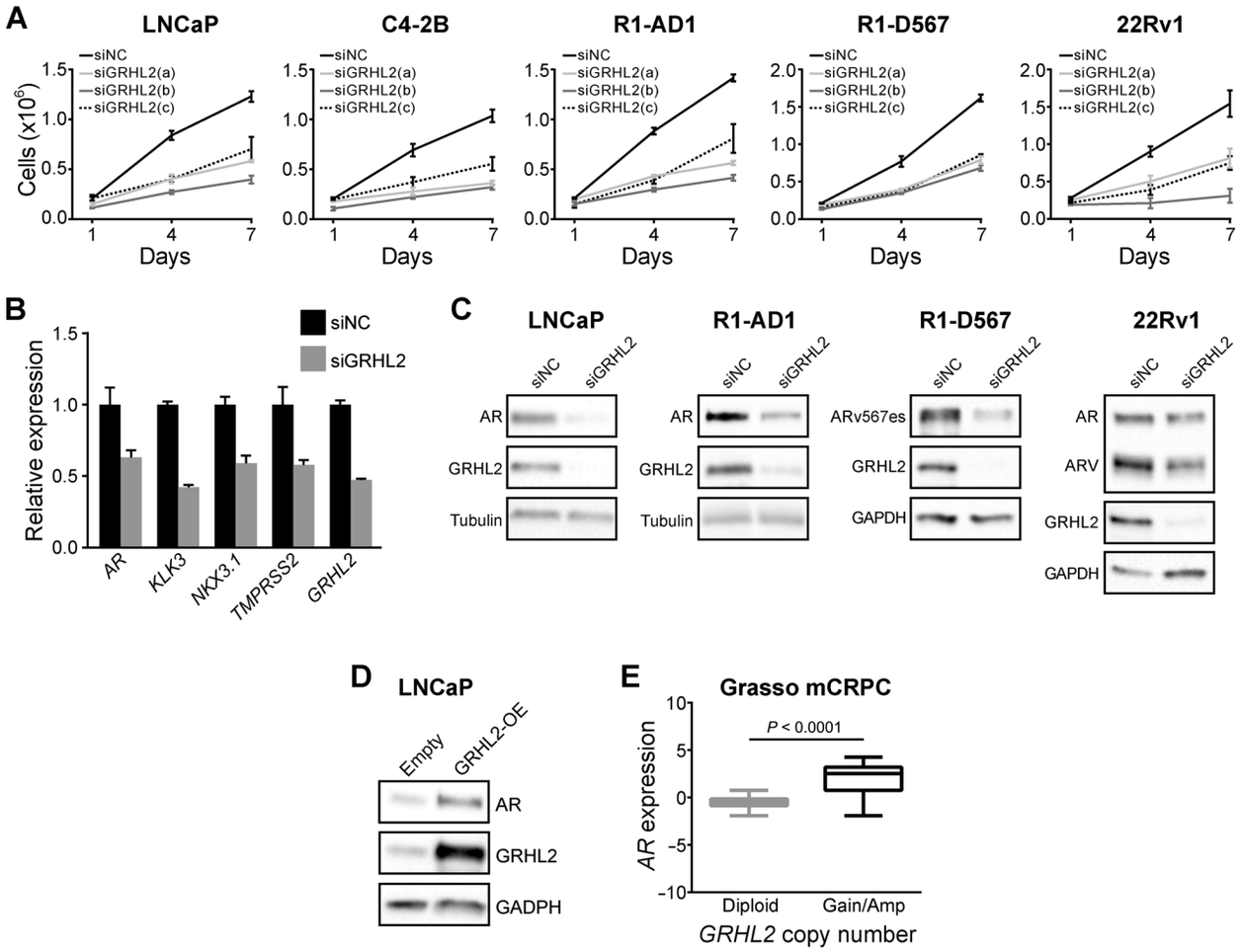

Figure 4.

Regulation of prostate cancer cell growth and AR expression and signaling by GRHL2. **A,** Prostate cancer cell lines were transfected with three distinct siRNAs and Trypan blue growth assays were performed. Error bars, ± SD. **B,** LNCaP cells were transfected with GRHL2 siRNA (siGRHL2) or a control (siNC), and gene expression was measured by RT-qPCR after 48 hours. Error bars, ± SEM of three independent experiments. **C,** Prostate cancer cell lines were transfected with GRHL2 siRNA (siGRHL2) or a control (siNC) and, 2 days later, protein expression was assessed by Western blotting. Tubulin or GAPDH are shown as loading controls. **D,** LNCaP cells were transfected with a GRHL2 expression vector (GRHL2-OE) or a control (Empty), and protein expression was assessed by Western blotting after 48 hours. GAPDH is shown as a loading control. **E,** *AR* expression is higher in metastatic CRPC (mCRPC) tumors with *GRHL2* copy-number gain or amplification compared with tumors with no change in *GRHL2* copy number (diploid). Data are from the Grasso cohort and were obtained via cBioPortal. *P* value was determined using an unpaired *t* test.

To evaluate whether AR-mediated regulation of *GRHL2* was direct, we examined ChIP-seq data for potential AR binding sites proximal to the *GRHL2* gene. In multiple AR cistromes derived from distinct cell line models of prostate cancer, we found evidence for AR (and ARV) binding near at two sites proximal to the *GRHL2* promoter (Supplementary Table S2). Both of these binding sites were also evident in a more recent study (35) examining the AR cistrome in clinical specimens (sites B and C in Fig. 3E); moreover, in this *in vivo* dataset, it was apparent that AR binding proximal to the *GRHL2* locus was notably increased in malignant compared with normal tissues (Fig. 3E). We validated AR binding at these sites by ChIP-qPCR in LNCaP cells (Fig. 3F). The tissue ChIP-seq data also suggested a weak AR binding event at the *GRHL2* promoter (Fig. 3E, site A), but this was not evident by ChIP-qPCR (Fig. 3F). Collectively, these data indicate that AR binds to multiple sites proximal to the *GRHL2* transcriptional start site, supporting a direct mode of transcriptional regulation.

GRHL2 promotes prostate cancer growth and is critical for AR expression

The functional role of GRHL2 in prostate cancer was assessed using siRNA-mediated knockdown. Three distinct GRHL2-targeted siRNAs, all of which were highly effective at silencing GRHL2 (Supplementary Fig. S2), caused inhibition of proliferation in multiple prostate cancer cell lines (Fig. 4A). Verifying the specificity of knockdown, none of the siRNAs inhibited the growth of GRHL2-negative PC-3 cells (Supplementary Fig. S3).

We subsequently tested the effect of a pool of the siRNAs (termed siGRHL2) on AR signaling. Knockdown of GRHL2 caused marked suppression of *AR* and AR target gene expression

(Fig. 4B) and decreased the levels of AR and ARV protein (Fig. 4C). Conversely, GRHL2 overexpression resulted in accumulation of AR protein (Fig. 4D). This latter finding is likely to be clinically relevant, because tumors with gain or amplification of *GRHL2* exhibited higher *AR* expression than diploid tumors (Fig. 4E).

We next assessed whether the physical association between GRHL2 and AR/ARV was a mechanism underlying GRHL2-mediated maintenance of AR/ARV expression. Following treatment with the protein biosynthesis inhibitor, cycloheximide, AR and ARV protein half-life was equivalent in siGRHL2 and control cells (Supplementary Fig. S4). These data suggest that maintenance of AR/ARV protein levels by GRHL2 is not primarily mediated by posttranslational mechanisms. By inference, we propose that the primary mechanism by which GRHL2 maintains AR/ARV protein levels is via induction of the *AR* gene.

Interplay between the transcriptional activities of AR and GRHL2

Given that RIME was designed to identify chromatin-associated protein:protein interactions, we speculated that GRHL2 could influence the transcriptional activity of AR. To test this hypothesis, we first evaluated the influence of GRHL2 on a well-characterized probasin reporter construct (13). For these experiments, we transiently expressed GRHL2 and AR in PC3 cells, which are negative for both factors: the rationale for this approach was that modulation of endogenous GRHL2 in AR-positive model systems resulted in downregulation of AR expression, which complicates assessment of transcriptional outcomes. GRHL2 modestly but reproducibly enhanced AR's transcriptional activity (Fig. 5A), indicating that it can act as a coactivator.

We subsequently used ChIP-seq to elucidate genome-wide AR and GRHL2 chromatin binding patterns in LNCaP cells with the aim of identifying potential sites of coordinate transcriptional regulation. The reads obtained across two ChIP-seq replicates for each protein were highly concordant, highlighting the robustness of the assay (Supplementary Fig. S5). Only peaks identified in both replicates were considered, yielding 5,378 GRHL2 and 1,202 AR high stringency binding sites. Comparison of the two cistromes revealed that 140 (11.6%) of AR binding sites were shared with GRHL2, highlighting potential for cooperative transcriptional regulation. Although not as extensive as the overlap between AR and the pioneer factors FoxA1 and GATA2 (21, 23, 36), the AR/GRHL2 overlap was highly significant compared with what would be expected by chance (Fisher exact test; P value = 3.40E–24). An example of a peak from each of the "AR-specific," "GRHL2-specific," and "shared" cistromes is shown in Fig. 4A. Quantitative analysis of tag density demonstrated the accuracy of these peak subsets (Supplementary Fig. S6).

Motif enrichment analysis of the cistromic data revealed strong enrichment for androgen response elements (ARE) and GRHL2 and FoxA1 motifs in the specific and shared peak subsets (Supplementary Table S3). Indeed, *de novo* motif generation identified a direct repeat of the FoxA1 motif as one of the most enriched sequences in the GRHL2-specific peak set (Fig. 5C). Supporting this finding, the GRHL2 cistrome overlapped substantially (25%–41%) with published LNCaP FoxA1 cistromes (Supplementary Fig. S7), an interaction that was experimentally validated in a recent study (37).

The AR and GRHL2 cistromes were assessed with respect to genomic features. The bulk of binding events in all three peak sets (AR-specific, GRHL2-specific, and shared) were located within introns and intergenic regions (Fig. 5D), although GRHL2-specific peaks also exhibited enrichment in gene promoters (2.78-fold over genomic average). Importantly, the shared GRHL2/AR binding events were highly enriched for epigenetic marks [K27-specific acetylation of histone 3 (H3K27ac) and K4-specific methylation of histone 3 (H3K4me2)], general transcription machinery (RNA-PII, Mediator), and transcription factors (FoxA1 and P300) that collectively demarcate enhancer sites and/or active transcription (Fig. 5E), indicating that colocation of these factors on chromatin promotes high transcriptional activity. Marks of transcription inhibition (H3K9me3 and H3K27me3) showed no enrichment at shared or factor-specific binding sites (Supplementary Fig. S8).

To further evaluate the relevance of shared AR/GRHL2 binding events in relation to transcriptional outputs, we identified genes with transcriptional start sites proximal to these sites to yield an "AR/GRHL2 cistrome-based signature" comprised of 194 genes. Importantly, this signature was elevated in clinical CRPC specimens and associated with a poor outcome following surgery, indicating that these genes are linked to prostate cancer progression (Fig. 5F). Moreover, by using GSEA and a published AR-responsive gene signature (23), we demonstrated that genes upregulated by AR were enriched near the shared AR/GRHL2 binding events (Supplementary Fig. S9), suggesting that colocalization of these factors on chromatin influences the androgenic transcriptional program. Collectively, these data indicate that GRHL2 and AR co-occupy a set of genomic loci associated with genes that are relevant in prostate cancer.

Elucidation of the GRHL2-regulated transcriptome in prostate cancer

To further explore the function of GRHL2 in prostate cancer, we used RNA-seq to measure transcriptional alterations in response to siGRHL2 in LNCaP cells. This analysis identified a GRHL2-regulated transcriptome comprised of 3,510 genes (Supplementary Table S4). GSEA was used to identify associations between the GRHL2 transcriptome and the "Hallmarks," "Reactome," and "Kegg" gene set collections of the Molecular Signature Database (Supplementary Table S5; ref. 29). Not unexpectedly, the hallmark most strongly enriched in genes downregulated by siGRHL2 was "androgen response" (Fig. 6A and Supplementary Table S5), further validating the critical requirement of GRHL2 for the AR signaling axis. Indeed, a signature of GRHL2 activity derived from the RNA-seq transcriptome was highly correlated with AR activity in both primary cancer and metastatic CRPC (Fig. 6B).

The finding that the majority of GRHL2 DNA binding events were independent of AR suggested that this transcription factor would have functions in prostate cancer beyond its critical role in the androgen signaling axis. To identify such functions, we considered other gene signatures enriched in the GRHL2-regulated transcriptome. Several consistent findings in response to loss of GRHL2 were observed (Supplementary Table S5), including: (i) downregulation of key pro-growth pathways, such as those regulated by ERBB2 (Fig. 6C), PI3K/Akt (Fig. 6D), and Hippo; (ii) downregulation of numerous biosynthetic pathways, most notably lipids, cholesterol, and steroids; (iii) upregulation of ribosomal genes; and (iv) downregulation of epithelial signatures and upregulation of epithelial–mesenchymal transition (EMT) signatures (Supplementary Fig. S10). We validated a subset of these biological associations. First, we demonstrated that loss of GRHL2 caused downregulation of *ERBB2* and other ERBB family

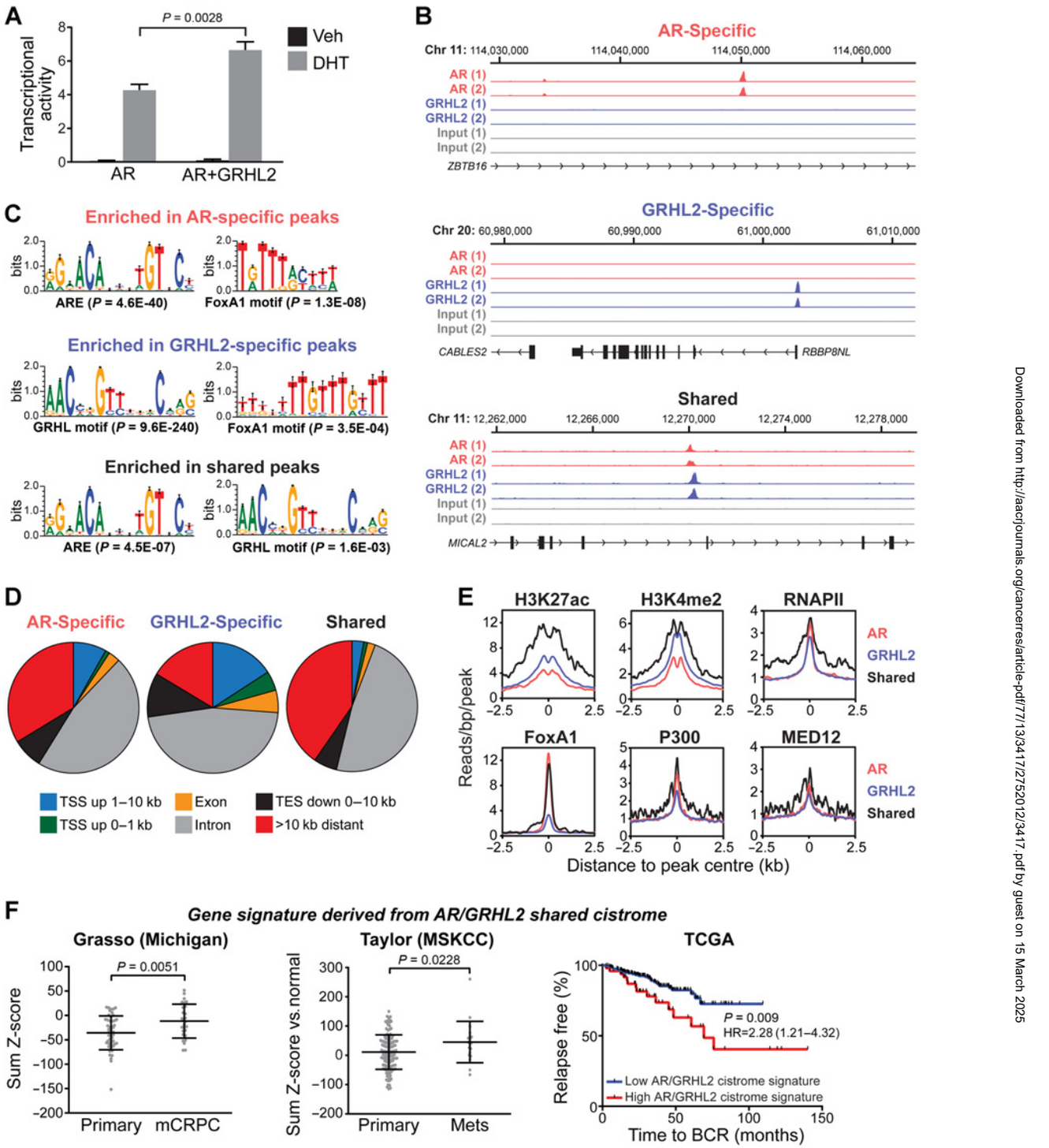

Figure 5.

GRHL2 enhances AR's transcriptional activity and associates with AR on chromatin. **A,** PC3 cells were transfected with plasmids expressing AR, GRHL2, and a probasin-derived AR-responsive reporter and subsequently treated with 1 nmol/L DHT or vehicle (Veh) control. Transcriptional activity values as assessed by luciferase assays represent the mean (±SEM) of six biological replicates; results are representative of three independent experiments. An unpaired *t* test was used to assess the effect of GRHL2 on AR activity. **B,** Examples of AR-specific, GRHL2-specific, and shared binding sites (left). **C,** Select motifs enriched in AR-specific, GRHL2-specific, and shared peaksets. Motifs were identified using a *de novo* Gibbs motif sampling approach. *P* values for enrichment over genomic background are shown. **D,** Genomic location summary of AR-specific, GRHL2-specific, and shared binding events. **E,** Distribution of normalized sequence tag density for H3K27ac, H3K4me2, RNAPII, FoxA1, P300, and Med12 in AR-specific, GRHL2-specific, and shared binding events. **F,** A gene signature based on shared GRHL2/AR binding events is upregulated in metastatic CRPC (two left plots) and associated with recurrence following radical prostatectomy (right plot).

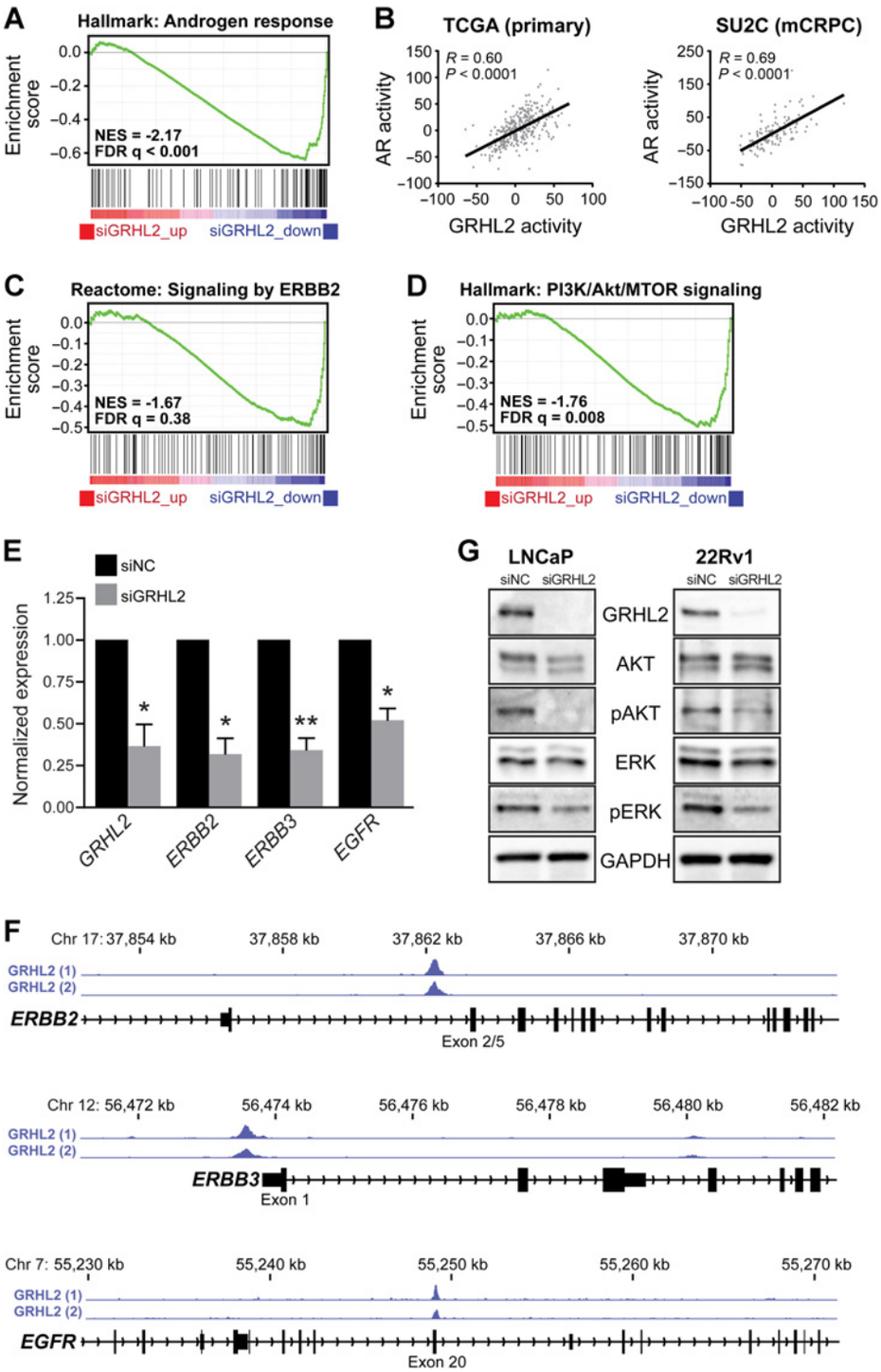

Figure 6.
GRHL2 regulates AR, ERBB, and PI3K/Akt signaling pathways. **A,** GRHL2 knockdown is associated with decreased expression of an AR-regulated gene set ("Hallmark: Androgen response"), as demonstrated by GSEA. **B,** Correlation between GRHL2- and AR-regulated gene signatures in primary prostate cancer (left, TCGA cohort) and metastatic CRPC (right, SU2C cohort). **C,** GRHL2 knockdown is associated with decreased expression of the PI3K/Akt pathway ("Hallmark: PI3K/Akt/MTOR signaling"), as demonstrated by GSEA. **D,** GRHL2 knockdown results in decreased expression of the ERBB2-regulated gene set ("Reactome: Signaling by ERBB2"), as demonstrated by GSEA. **E,** GRHL2 knockdown (siGRHL2) leads to reduced expression of *ERBB2, ERBB3,* and *EGFR*. Values for the negative control (siNC) were set to 1, and error bars are ± SEM. *P* values were determined using one-sample *t* tests (*, $P < 0.05$; **, $P < 0.01$). **F,** GRHL2 binding events in LNCaP cells, identified by ChIP-seq, proximal to *ERBB2, ERBB3,* and *EGFR*. **G,** GRHL2 knockdown results in decreased phosphorylation of Akt (pAkt) and ERK (pERK) in LNCaP and 22Rv1 cells, as assessed by Western blotting.

members *ERBB3* and *EGFR* (Fig. 6E), likely due to the capacity of GRHL2 to directly regulate these genes (Fig. 6F; ref. 38). Second, we observed a significant decrease in active components of the PI3K/Akt pathway (i.e., phosphorylated Akt and ERK) following GRHL2 knockdown (Fig. 6G). Finally, we validated the potent anti-EMT and anti-invasive activity of GRHL2 both *in vitro* and *in vivo* (below).

Loss of GRHL2 promotes EMT and invasion

EMT has been demonstrated to play a key role in certain phases of metastasis, including escape from the primary tumor, migration and invasion into the stroma, entry/exit from the bloodstream, and suppression of senescence, apoptosis, and anoikis (39). With this in mind, we hypothesized that the negative association between GRHL2 and EMT revealed by our RNA-seq

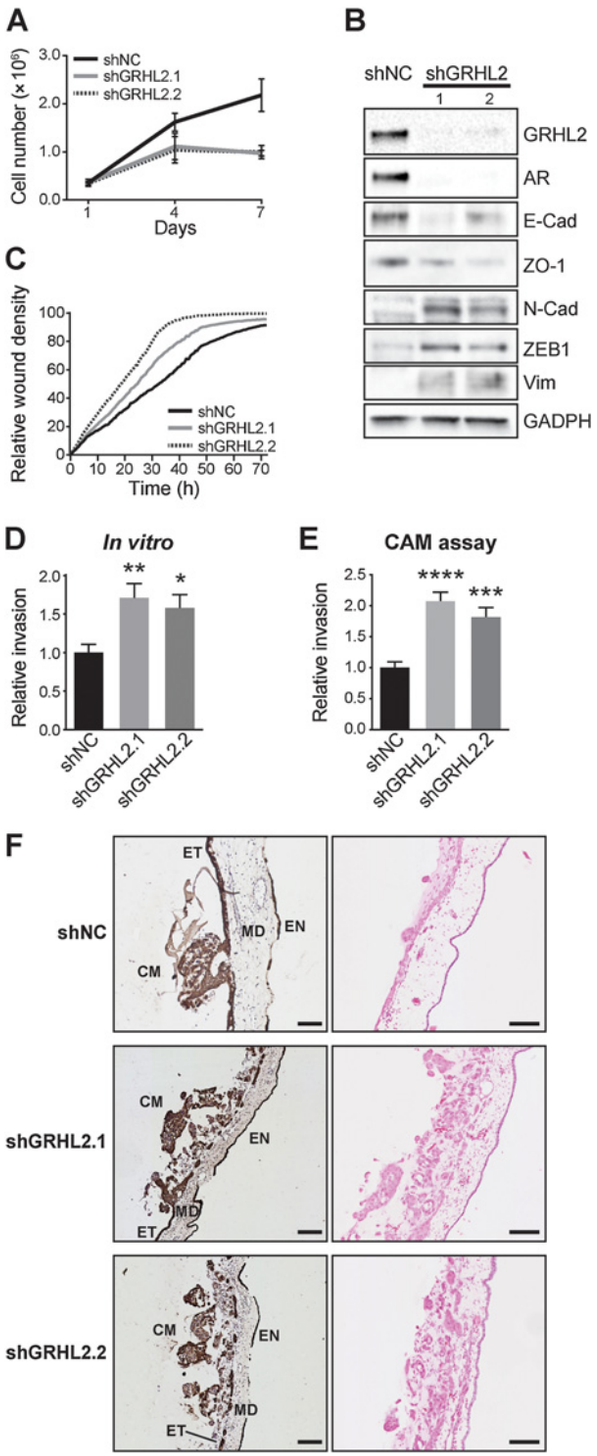

Figure 7.

GRHL2 suppresses EMT and invasion of prostate cancer. **A,** The growth of two distinct clones with stable knockdown of GRHL2 (shGRHL2.1 and shGRHL2.2) was compared with a control (shNC) in Trypan blue growth assays. Error bars, ± SD. **B,** Stable knockdown of GRHL2 decreases epithelial marker (E-cad, ZO-1) and increases mesenchymal marker (N-cad, ZEB1, Vim) expression at the protein level in LNCaP cells. E-cad, E-cadherin; N-cad, N-cadherin; Vim, vimentin. **C,** Stable knockdown of GRHL2 increases migration of LNCaP cells in a scratch-wound assay. **D,** Stable knockdown of GRHL2 increases invasion of LNCaP cells. Values for the negative control (NC) were set to 1, and error bars are ± SEM. *P* values were determined using unpaired *t* tests (**, $P < 0.01$). **E,** Stable knockdown of GRHL2 promotes cancer cell invasion in CAM assays. Data represent the mean percentage of images with into the mesoderm ± SEM. *P* value was determined using an unpaired two-sided *t* test (***, $P < 0.001$; ****, $P < 0.0001$). **F,** Representative images from the CAM assays. Cancer cell:Matrigel grafts (CM) were placed on top of the ectoderm (ET) layer and cancer cell invasion into the CAM mesoderm (MD) was assessed in day 14 chick embryos. Endoderm, EN. Shown are cytokeratin (CK) IHC (left) and hematoxylin and eosin (right) images. Scale bars, 100 μm.

data (Supplementary Fig. S10) could have important biological ramifications.

To address this hypothesis, we generated LNCaP cells with stable knockdown of GRHL2 using two distinct lentiviral shRNA constructs. Recapitulating the short-term siRNA experiments, GRHL2 silencing resulted in a reduced growth rate and a dramatic decrease in AR expression (Fig. 7A and B). To examine how loss of GRHL2 influences the epithelial phenotype, the expression of epithelial and mesenchymal markers was measured by Western blotting in the LNCaP-shGRHL2 cells. As expected, knockdown of GRHL2 caused loss of epithelial and gain of mesenchymal factors, indicative of EMT (Fig. 7B).

Recent studies have elucidated transcriptional targets via which GRHL2 suppresses EMT in breast and ovarian cancer (38, 40). For example, GRHL2 binds to promoter and/or enhancer elements to directly activate *CDH1* (E-cadherin), *TJP1* (ZO-1), *CLDN4*, *ELF3*, *EPCAM*, and *RAB25*, thereby promoting an epithelial phenotype. Analysis of our ChIP-seq data revealed that GRHL2 also associates with these cis-regulatory elements in LNCaP cells (Supplementary Fig. S11), suggesting that the transcriptional targets via which GRHL2 fosters epithelial identity are concordant among distinct cancer types.

To investigate the phenotypic consequences of GRHL2-regulated EMT, we evaluated motility and invasion of the LNCaP-shGRHL2 cells using three distinct assays. We first used a scratch wound assay and found that stable knockdown of GRHL2 significantly enhanced cell migration (Fig. 7C). Subsequently, an *in vitro* transwell assay was employed to measure cell invasion through Matrigel, which mimics basement membrane. As expected, LNCaP-shGRHL2 cells were markedly more invasive than control cells (Fig. 7D). Finally, the invasive capacity of the modified cell lines was evaluated in a more physiologically relevant setting using a CAM assay (41), which allows visualization of cell invasion through an ectoderm into mesoderm. Cancer cell/Matrigel grafts were implanted onto the CAM, and, after 3 days, invasion was assessed by pan-cytokeratin immunohistochemistry. Control LNCaP cells invaded through the ectoderm of the CAM very poorly (Fig. 7E and F). By contrast, knockdown of GRHL2 greatly enhanced the capacity of LNCaP cells to disrupt the ectodermal layer and invade into the mesoderm (Fig. 7E and F).

To evaluate the generalizability of these findings, we conducted experiments in another model system, 22Rv1. In these experiments, cells were transfected with siGRHL2 to determine whether acute loss of GRHL2 was sufficient to promote EMT. As expected, transient knockdown of GRHL2 resulted in EMT within 2 days (Supplementary Fig. S12). This experiment suggests that maintenance of epithelial status by GRHL2 is a general phenomenon in prostate cancer and that loss of GRHL2

could rapidly enhance mesenchymal, pro-invasive characteristics of tumor cells.

Discussion

Using a powerful and unbiased proteomic technique, we have identified GRHL2 as a new binding partner of AR, the key driver of prostate cancer. Our data indicate that GRHL2 has a dichotomous oncogenic/protective role in this disease: it can act as an oncogene by enhancing AR signaling and promoting cancer cell proliferation; alternatively, it can potently suppress cancer cell EMT and invasion, phenotypes that are associated with disease progression and metastasis.

GRHL2 is a member of the Grainyhead-like family of transcription factors, which are expressed primarily in epithelia in a tissue- and developmental-specific manner and are critical for organogenesis, epidermal development, and wound healing (42). More recently, a role for GRHL2 in various solid cancers has been proposed, although its precise functions are largely unknown. Increased GRHL2 expression is associated with poor outcomes in liver, kidney, gastric, and colorectal cancers, and experimental studies have revealed that it can promote growth of certain cancer models *in vitro* and *in vivo* (42). By contrast, the action of GRHL2 in breast cancer is somewhat controversial, with studies purporting to demonstrate both oncogenic and tumor-suppressive activities (43, 44). A putative explanation for this apparent discrepancy was provided by Werner and colleagues, who presented evidence for dual functionality of GRHL2 in breast cancer: namely, it can both promote tumor growth but suppress EMT (38). Herein, we have shown that GRHL2 plays an analogous dual role in prostate cancer growth and progression. The spatiotemporality of GRHL2 expression and activity in prostate (and breast) tumors is likely to be critical in dictating which of these roles dominate. More specifically, in early, localized tumors, GRHL2 would act to promote cancer growth; however, as disease progressed, GRHL2 could act to suppress EMT and thereby curb stromal invasion, intravasation, and survival of circulating tumor cells, with the collective outcome being inhibition of metastasis; finally, in micrometastases, GRHL2 could revert to an oncoprotein by reversing mesenchymal phenotypes, re-activating proliferation, and facilitating establishment of clinically significant metastases. Recent work suggests that dual functionality of GRHL2 (i.e., growth-promoting but EMT/invasion-suppressing) could be a generalizable phenomenon in carcinomas (40, 45).

The data presented herein demonstrate that the relationship between GRHL2 and the AR signaling axis is multifaceted and complex. More specifically, GRHL2 is not only essential for the maintenance of AR expression, but also acts as an AR transcriptional coactivator. With regards to the latter function, it must be noted that GRHL2 and AR share only a small proportion of their respective cistromes. However, these shared binding events occur proximal to a set of genes that are relevant in prostate cancer. These critical roles for GRHL2 in the AR signaling axis are particularly relevant in light of our finding that *GRHL2* is a direct AR target gene. Reciprocal regulation creates a potent positive feed-forward loop between AR and GRHL2, which may be amplified further in the CRPC setting where the genes encoding both factors are commonly amplified and/or upregulated.

A key function of the AR signaling axis in both the normal and malignant prostate is to regulate epithelial differentiation (46, 47). The work reported herein provides new insight into molecular mechanisms underlying this function: specifically, by directly promoting GRHL2 expression, AR indirectly activates a transcriptional program comprising key epithelial identity factors such as *CDH1* (E-cadherin), *TJP1* (ZO-1), *ELF3*, *CLDN4*, and *EPCAM*. Interestingly, by interrogating AR chromatin binding events in prostate tumors (35), we found evidence that it could directly regulate a subset of these genes in concert with GRHL2 (Supplementary Fig. S11). Further investigation of the cistromic interplay between these two factors, including in the normal prostate, is required to definitively identify their shared target genes.

There is an urgent requirement for novel strategies that inhibit growth of CRPC and improve patient outcomes; one such strategy that has been proposed is targeting transcriptional coregulators rather than AR itself. In this context, our study is significant because it identifies a critical new coregulator that not only enhances AR activity but is also essential for the maintenance of AR expression. However, although targeting GRHL2 could disable the AR signaling axis at multiple levels, it may concomitantly enhance the metastatic capacity of the tumor. As such, if strategies to inhibit GRHL2 were developed, their application in prostate cancer would require careful consideration.

Disclosure of Potential Conflicts of Interest

G.V. Raj has received honoraria from the speakers bureau of Astellas, Medivation, and Sanofi. S.R. Plymate reports receiving commercial research grant from Johnson and Johnson and is a consultant/advisory board member for ESSA Pharma. No potential conflicts of interest were disclosed by the other authors.

Authors' Contributions

Conception and design: S. Paltoglou, T.E. Hickey, I. Coutinho, G.V. Raj, W.D. Tilley, L.A. Selth

Development of methodology: S. Paltoglou, R. Das, T.E. Hickey, L.A. Selth

Acquisition of data (provided animals, acquired and managed patients, provided facilities, etc.): S. Paltoglou, R. Das, S.L. Townley, T.E. Hickey, G.A. Tarulli, A.R. Hanson, I. Denis, J.S. Carroll, S.R. Plymate, L.A. Selth

Analysis and interpretation of data (e.g., statistical analysis, biostatistics, computational analysis): S. Paltoglou, R. Das, S.L. Townley, G.A. Tarulli, I. Denis, S.M. Dehm, G.V. Raj, S.R. Plymate, W.D. Tilley, L.A. Selth

Writing, review, and/or revision of the manuscript: S. Paltoglou, T.E. Hickey, J.S. Carroll, S.M. Dehm, G.V. Raj, S.R. Plymate, W.D. Tilley, L.A. Selth

Administrative, technical, or material support (i.e., reporting or organizing data, constructing databases): S. Paltoglou, R. Fernandes, A.R. Hanson, L.A. Selth

Study supervision: S. Paltoglou, W.D. Tilley, L.A. Selth

Acknowledgments

The authors thank Drs. Colm Morrisey, Larry True, and Tony Rizzardi (University of Washington) for assistance with the prostate cancer tissue microarray, Drs. Clive D'Santos, Chris Taylor, and Eva Papachristou from the Cancer Research UK Cambridge Institute Proteomics Core Facility for expert assistance with RIME, Mark Van der Hoek from the South Australian Health and Medical Research Institute Genomics Facility for assistance with ChIP-seq and RNA-seq, and Dr. Nicholas Mitsiades (Baylor College of Medicine) for sharing unpublished data. The results published here are in part based on data generated by TCGA, established by the NCI and the National Human Genome Research Institute, and we are grateful to the specimen donors and relevant research groups associated with this project.

Grant Support

This work was supported by funding from the National Health and Medical Research Council of Australia (ID 1008349 to W.D. Tilley; ID

1083961 to L.A. Selth and W.D. Tilley), a Prostate Cancer Research Programs Transformative Impact Award from the US Department of Defense (W81XWH-13-2-0093 to S.R. Plymate, W.D. Tilley, G.V. Raj, S.M. Dehm, and L.A. Selth), and NIH grant R01CA174777 (S.M. Dehm). L.A. Selth was supported by a Young Investigator Award from the Prostate Cancer Foundation (Foundation 14 award).

The costs of publication of this article were defrayed in part by the payment of page charges. This article must therefore be hereby marked *advertisement* in accordance with 18 U.S.C. Section 1734 solely to indicate this fact.

Received June 14, 2016; revised August 26, 2016; accepted April 20, 2017; published OnlineFirst May 4, 2017.

References

1. Mitsiades N. A road map to comprehensive androgen receptor axis targeting for castration-resistant prostate cancer. Cancer Res 2013; 73:4599–605.
2. Wyatt AW, Gleave ME. Targeting the adaptive molecular landscape of castration-resistant prostate cancer. EMBO Mol Med 2015;7:878–94.
3. Chmelar R, Buchanan G, Need EF, Tilley W, Greenberg NM. Androgen receptor coregulators and their involvement in the development and progression of prostate cancer. Int J Cancer 2007;120:719–33.
4. Mohammed H, Taylor C, Brown GD, Papachristou EK, Carroll JS, D'Santos CS. Rapid immunoprecipitation mass spectrometry of endogenous proteins (RIME) for analysis of chromatin complexes. Nat Protoc 2016;11: 316–26.
5. Nyquist MD, Li Y, Hwang TH, Manlove LS, Vessella RL, Silverstein KA, et al. TALEN-engineered AR gene rearrangements reveal endocrine uncoupling of androgen receptor in prostate cancer. Proc Natl Acad Sci U S A 2013;110:17492–7.
6. Chan SC, Selth LA, Li Y, Nyquist MD, Miao L, Bradner JE, et al. Targeting chromatin binding regulation of constitutively active AR variants to overcome prostate cancer resistance to endocrine-based therapies. Nucleic Acids Res 2015;43:5880–97.
7. Das R, Gregory PA, Fernandes RC, Denis I, Wang Q, Townley SL, et al. MicroRNA-194 promotes prostate cancer metastasis by inhibiting SOCS2. Cancer Res 2017;77:1021–34.
8. Gao J, Aksoy BA, Dogrusoz U, Dresdner G, Gross B, Sumer SO, et al. Integrative analysis of complex cancer genomics and clinical profiles using the cBioPortal. Sci Signal 2013;6:pl1.
9. Selth LA, Das R, Townley SL, Coutinho I, Hanson AR, Centenera MM, et al. A ZEB1-miR-375-YAP1 pathway regulates epithelial plasticity in prostate cancer. Oncogene 2017;36:24–34.
10. Tarulli GA, De Silva D, Ho V, Kunasegaran K, Ghosh K, Tan BC, et al. Hormone-sensing cells require Wip1 for paracrine stimulation in normal and premalignant mammary epithelium. Breast Cancer Res 2013;15:R10.
11. Hickey TE, Irvine CM, Dvinge H, Tarulli GA, Hanson AR, Ryan NK, et al. Expression of androgen receptor splice variants in clinical breast cancers. Oncotarget 2015;6:44728–44.
12. Rizzardi AE, Rosener NK, Koopmeiners JS, Isaksson Vogel R, Metzger GJ, Forster CL, et al. Evaluation of protein biomarkers of prostate cancer aggressiveness. BMC Cancer 2014;14:244.
13. Gillis JL, Selth LA, Centenera MM, Townley SL, Sun S, Plymate SR, et al. Constitutively-active androgen receptor variants function independently of the HSP90 chaperone but do not confer resistance to HSP90 inhibitors. Oncotarget 2013;4:691–704.
14. Schmidt D, Wilson MD, Spyrou C, Brown GD, Hadfield J, Odom DT. ChIP-seq: Using high-throughput sequencing to discover protein-DNA interactions. Methods 2009;48:240–8.
15. Zhu LJ, Gazin C, Lawson ND, Pages H, Lin SM, Lapointe DS, et al. ChIPpeakAnno: A Bioconductor package to annotate ChIP-seq and ChIP-chip data. BMC Bioinformatics 2010;11:237.
16. Liu T, Ortiz JA, Taing L, Meyer CA, Lee B, Zhang Y, et al. Cistrome: An integrative platform for transcriptional regulation studies. Genome Biol 2011;12:R83.
17. Heinz S, Benner C, Spann N, Bertolino E, Lin YC, Laslo P, et al. Simple combinations of lineage-determining transcription factors prime cis-regulatory elements required for macrophage and B cell identities. Mol Cell 2010;38:576–89.
18. Ji H, Jiang H, Ma W, Johnson DS, Myers RM, Wong WH. An integrated software system for analyzing ChIP-chip and ChIP-seq data. Nat Biotechnol 2008;26:1293–300.
19. Need EF, Selth LA, Trotta AP, Leach DA, Giorgio L, O'Loughlin MA, et al. The unique transcriptional response produced by concurrent estrogen and progesterone treatment in breast cancer cells results in upregulation of growth factor pathways and switching from a Luminal A to a Basal-like subtype. BMC Cancer 2015;15:791.
20. Robinson JT, Thorvaldsdottir H, Winckler W, Guttman M, Lander ES, Getz G, et al. Integrative genomics viewer. Nat Biotechnol 2011;29:24–6.
21. Wang D, Garcia-Bassets I, Benner C, Li W, Su X, Zhou Y, et al. Reprogramming transcription by distinct classes of enhancers functionally defined by eRNA. Nature 2011;474:390–4.
22. Yu J, Yu J, Mani RS, Cao Q, Brenner CJ, Cao X, et al. An integrated network of androgen receptor, polycomb, and TMPRSS2-ERG gene fusions in prostate cancer progression. Cancer Cell 2010;17:443–54.
23. He B, Lanz RB, Fiskus W, Geng C, Yi P, Hartig SM, et al. GATA2 facilitates steroid receptor coactivator recruitment to the androgen receptor complex. Proc Natl Acad Sci U S A 2014;111:18261–6.
24. Trapnell C, Pachter L, Salzberg SL. TopHat: Discovering splice junctions with RNA-Seq. Bioinformatics 2009;25:1105–11.
25. Blankenberg D, Von Kuster G, Coraor N, Ananda G, Lazarus R, Mangan M, et al. Galaxy: A web-based genome analysis tool for experimentalists. Curr Protoc Mol Biol 2010;Chapter 19:Unit 19 10 1–21.
26. Giardine B, Riemer C, Hardison RC, Burhans R, Elnitski L, Shah P, et al. Galaxy: A platform for interactive large-scale genome analysis. Genome Res 2005;15:1451–5.
27. Anders S, Pyl PT, Huber W. HTSeq–a Python framework to work with high-throughput sequencing data. Bioinformatics 2015;31:166–9.
28. Anders S, Huber W. Differential expression analysis for sequence count data. Genome Biol 2010;11:R106.
29. Subramanian A, Tamayo P, Mootha VK, Mukherjee S, Ebert BL, Gillette MA, et al. Gene set enrichment analysis: A knowledge-based approach for interpreting genome-wide expression profiles. Proc Natl Acad Sci U S A 2005;102:15545–50.
30. Cancer Genome Atlas Research Network. Electronic address scmo, Cancer Genome Atlas Research N. The Molecular Taxonomy of Primary Prostate Cancer. Cell 2015;163:1011–25.
31. Grasso CS, Wu YM, Robinson DR, Cao X, Dhanasekaran SM, Khan AP, et al. The mutational landscape of lethal castration-resistant prostate cancer. Nature 2012;487:239–43.
32. Taylor BS, Schultz N, Hieronymus H, Gopalan A, Xiao Y, Carver BS, et al. Integrative genomic profiling of human prostate cancer. Cancer Cell 2010;18:11–22.
33. Rajan P, Sudbery IM, Villasevil ME, Mui E, Fleming J, Davis M, et al. Next-generation sequencing of advanced prostate cancer treated with androgen-deprivation therapy. Eur Urol 2014;66:32–9.
34. Sharma NL, Massie CE, Ramos-Montoya A, Zecchini V, Scott HE, Lamb AD, et al. The androgen receptor induces a distinct transcriptional program in castration-resistant prostate cancer in man. Cancer Cell 2013;23:35–47.
35. Pomerantz MM, Li F, Takeda DY, Lenci R, Chonkar A, Chabot M, et al. The androgen receptor cistrome is extensively reprogrammed in human prostate tumorigenesis. Nat Genet 2015;47:1346–51.
36. Sahu B, Laakso M, Ovaska K, Mirtti T, Lundin J, Rannikko A, et al. Dual role of FoxA1 in androgen receptor binding to chromatin, androgen signalling and prostate cancer. EMBO J 2011;30:3962–76.
37. Jozwik KM, Chernukhin I, Serandour AA, Nagarajan S, Carroll JS. FOXA1 directs H3K4 monomethylation at enhancers via recruitment of the methyltransferase MLL3. Cell Rep 2016;17:2715–23.
38. Werner S, Frey S, Riethdorf S, Schulze C, Alawi M, Kling L, et al. Dual roles of the transcription factor grainyhead-like 2 (GRHL2) in breast cancer. J Biol Chem 2013;288:22993–3008.
39. De Craene B, Berx G. Regulatory networks defining EMT during cancer initiation and progression. Nat Rev Cancer 2013;13:97–110.
40. Chung VY, Tan TZ, Tan M, Wong MK, Kuay KT, Yang Z, et al. GRHL2-miR-200-ZEB1 maintains the epithelial status of ovarian cancer through transcriptional regulation and histone modification. Sci Rep 2016;6:19943.

41. Lokman NA, Elder AS, Ricciardelli C, Oehler MK. Chick chorioallantoic membrane (CAM) assay as an in vivo model to study the effect of newly identified molecules on ovarian cancer invasion and metastasis. Int J Mol Sci 2012;13:9959–70.
42. Mlacki M, Kikulska A, Krzywinska E, Pawlak M, Wilanowski T. Recent discoveries concerning the involvement of transcription factors from the Grainyhead-like family in cancer. Exp Biol Med (Maywood) 2015;240: 1396–401.
43. Cieply B, Riley Pt, Pifer PM, Widmeyer J, Addison JB, Ivanov AV, et al. Suppression of the epithelial-mesenchymal transition by Grainyhead-like-2. Cancer Res 2012;72:2440–53.
44. Xiang X, Deng Z, Zhuang X, Ju S, Mu J, Jiang H, et al. Grhl2 determines the epithelial phenotype of breast cancers and promotes tumor progression. PLoS One 2012;7:e50781.
45. Chen W, Yi JK, Shimane T, Mehrazarin S, Lin YL, Shin KH, et al. Grainyhead-like 2 regulates epithelial plasticity and stemness in oral cancer cells. Carcinogenesis 2016;37:500–10.
46. Das R, Gregory PA, Hollier BG, Tilley WD, Selth LA. Epithelial plasticity in prostate cancer: Principles and clinical perspectives. Trends Mol Med 2014;20:643–51.
47. Nieto CM, Rider LC, Cramer SD. Influence of stromal-epithelial interactions on androgen action. Endocr Relat Cancer 2014;21:T147–60.